Cell

Plasmodium Circumsporozoite Protein Promotes the Development of the Liver Stages of the Parasite

Agam Prasad Singh,[1,*] Carlos A. Buscaglia,[1] Qian Wang,[1] Agata Levay,[3] Daniel R. Nussenzweig,[3] John R. Walker,[4] Elizabeth A. Winzeler,[4,5] Hodaka Fujii,[1,2] Beatriz M.A. Fontoura,[3,6] and Victor Nussenzweig[1,6]
[1]Department of Pathology
[2]NYU Cancer Institute
New York University School of Medicine, New York, NY 10016, USA
[3]Department of Cell Biology, University of Texas Southwestern Medical Center, Dallas, TX 75390, USA
[4]Genomics Institute of the Novartis Research Foundation, San Diego, CA 92037, USA
[5]Department of Cell Biology, ICND202 The Scripps Research Institute La Jolla, CA 92037, USA
[6]These authors contributed equally to this work.
*Correspondence: singha05@med.nyu.edu
DOI 10.1016/j.cell.2007.09.013

SUMMARY

The liver stages of malaria are clinically silent but have a central role in the *Plasmodium* life cycle. Liver stages of the parasite containing thousands of merozoites grow inside hepatocytes for several days without triggering an inflammatory response. We show here that Plasmodium uses a PEXEL/VTS motif to introduce the circumsporozoite (CS) protein into the hepatocyte cytoplasm and a nuclear localization signal (NLS) to enter its nucleus. CS outcompetes NFκB nuclear import, thus downregulating the expression of many genes controlled by NFκB, including those involved in inflammation. CS also influences the expression of over one thousand host genes involved in diverse metabolic processes to create a favorable niche for the parasite growth. The presence of CS in the hepatocyte enhances parasite growth of the liver stages in vitro and in vivo. These findings have far reaching implications for drug and vaccine development against the liver stages of the malaria parasite.

INTRODUCTION

Malaria infection is initiated by injection of *Plasmodium* sporozoites by mosquitoes into the host. Sporozoites rapidly home in the liver, invade hepatocytes where they develop in the cytoplasm inside a parasitophorous vacuole (PV), and grow into a schizont containing 10,000–30,000 merozoites. The liver stages, named exo-erythrocytic forms (EEFs), take several days to fully mature and release merozoites into the blood where they start the erythrocytic cycle. The biology of EEFs is mostly unknown, in part because they are very few in number, and difficult to isolate from the bulk of uninfected liver cells.

Plasmodium sporozoites are covered with a surface protein known as circumsporozoite (CS) protein. CS also covers the plasma membrane of EEFs and has been detected in the cytoplasm of the infected hepatocytes (Hollingdale et al., 1983). Between 12-24 hr after invasion CS is associated with the outer rim of the hepatocyte nucleus (Hugel et al., 1996). However, it is not known how CS (Mr. ~40,000 Da) manages to traverse the membrane of the PV that is impermeable to the passage of macromolecules larger than 1400 Da (Desai and Rosenberg, 1997). *Plasmodium* blood stages also reside inside a PV, and some parasite proteins are exported to the erythrocyte cytoplasm. Most exported molecules contain, in the N-terminus, a motif denominated pexel (*p*lasmodium *ex*port *el*ement) (Marti et al., 2004) or VTS (*v*acuolar *t*ranslocation *s*ignal) (Hiller et al., 2004).

The entry of CS in the cytoplasm is paradoxical because CS is processed and presented on the surface of the hepatocytes where it is recognized by cytotoxic T cells (CTL). Recent studies show in fact that CS is an immunodominant protective T cell antigen (Kumar et al., 2006), raising the obvious question of why the parasite facilitates its demise. On the basis of an observation that CS inhibits in vitro translation it has been suggested that CS inhibits protein synthesis in infected hepatocytes (Frevert et al., 1998). It was implied that this would block antigen presentation and parasite uses this as immune evasion mechanism. Recently a transgenic mouse constitutively expressing CS was created. If CS has ribo-toxic effects as suggested by previous study, one would expect at least some defect in CS transgenic mouse, however CS-transgenic mouse did not show any defect (Kumar et al., 2006). Fully grown EEFs occupy as much as 2/3 of the total hepatocyte cytoplasm, and some of the primate species reside in the liver for more than a week without signs of

apoptosis (van de Sand et al., 2005) in the host cell, or of inflammatory responses surrounding it (Short et al., 1954).

In this paper we study the function of CS in the cytoplasm of the liver cells using two rodent malaria parasites, *P. berghei* and *P. yoelii* that share most biological properties. We show that CS elicits profound changes in the transcriptional program of the host cell to the parasite's benefit.

RESULTS

The Pexel/VTS Motifs of CS Are Functional

The amino acid sequence alignment of the CS N-terminus from *Plasmodium* species reveals the presence of two typical pexel/VTS motifs, except that CS from *P. vivax* and related monkey malaria species have only one motif (Figure 1A). To determine whether these putative pexel motifs are functional we transiently transfected *P. berghei* schizonts with a plasmid encoding the amino terminal region (amino acids 1–74) of *P. berghei* CS fused to GFP (Figure 1B). The analysis by fluorescence microscopy of live blood stage parasites showed that the fusion protein entered the red blood cell cytoplasm (Figure 1C, WT). To identify which one of the two putative pexel/VTS motifs of *P. berghei* CS is required for PV translocation, we mutated the critical arginine and leucine residue of each of the two motifs to alanine. Figure 1C shows that both motifs are functional, and that the export of CS is aborted only when both motifs were mutated.

Pexel Mutant EEFs Are Defective in CS Export to the Hepatocyte Cytoplasm

Based on the findings above, we targeted both pexel/VTS motifs in full length CS, and obtained a stable mutant parasite by the double crossover method (Menard and Janse, 1997). The schematic representations of the knockout construct and of the expected mutant parasites are shown in Figures 2A and 2B. Upon restriction digestion of the genomic DNA from wild-type and mutant parasite with *Eco*R V, the expected fragments were 4.0 kb for the wild-type and 7.2 kb for the mutant. Analysis of genomic DNA from the wild-type and cloned mutant parasite confirmed the integration event (Figure 2B). Sequencing of a PCR fragment, comprising the CS gene obtained from the genomic DNA of parasite, confirmed the presence of the expected mutation. *Pst I* and *Sac* I sites were incorporated next to the sites of the mutation. Digestion of the PCR product obtained from the mutant genomic DNA, with *Pst I* and *Sac* I enzymes, provides additional evidence for the presence of the mutation (data not shown).

Next, we fed mosquitoes with the blood stages of the CS pexel/VTS double mutant parasites. The development of the mutant and wild-type parasites in the mosquitoes were then analyzed on days fourteen and eighteen postinfection for the number of oocyst and salivary gland sporozoites, respectively. In the mosquito stages, the development of the CS pexel/VTS double mutant was similar to that of the transfected wild-type. On day 14 the number of oocyst/mosquito was 40 ± 10 (n = 3) for the mutant and 50 ± 15 (n = 3) for the wild-type; the number of oocyst sporozoites/mosquito was 37,000 ± 3,000 (n = 3) for the mutant and 40,000 ± 5,000 (n = 3) for the wild-type; and on day 18 the number of sporozoites/salivary gland was 13,000 ± 2,000 (n = 5) for the mutant and 15,000 ± 4,000 (n = 5) for wild-type. By light microscopy, the CS pexel/VTS mutant sporozoites were indistinguishable from transfected wild-type. The gliding motility patterns were similar in both mutant and wild-type (Figure S1A in the Supplemental Data available with this article online). In wild-type sporozoites, the CS protein is cleaved at the N-terminal by a parasite cysteine protease, and this processing is required for parasite infectivity (Coppi et al., 2005). Although several substitutions were introduced in the amino terminus of the pexel/VTS of the CS mutants, the protein was processed correctly (Figure S1B). In short, we did not detect any abnormality in the mosquito stages of the pexel/VTS mutant sporozoites.

We then compared the abilities of the mutants and wild-type salivary gland sporozoites to invade and complete the cycle in HepG2 cells. We found no significant differences in the invasion ability of the two parasites. In 500 events counted, mutant and wild-type parasites inside HepG2 cells were 47 ± 3% and 48 ± 3%, respectively. We then analyzed the infected cells for the presence of CS in the cytoplasm between one to three hours after sporozoite invasion when the presence of cytoplasmic CS is at a peak. While CS was found in the cytoplasm of every HepG2 cells infected with wild-type sporozoites, CS cytoplasmic staining was absent in 90% or more of cells infected with the mutants (Figures 2C and 2D). We conclude that the pexel/VTS motifs of CS are required for crossing the PV membrane.

Pexel/VTS Mutant EEFs Are Defective in Development

Although the infectivity of the pexel/VTS mutant parasite is indistinguishable from the wild-type, the mutation was associated with a profound developmental inhibition of EEFs. At forty-eight hours post infection, when the EEFs are close to their maximum size, the amount of parasite-specific ribosomal RNAs (rRNA) in the rat liver was 14 ± 3 times lower in mutants than in the wild-type (Figure 2E). We also compared numbers and sizes of the EEFs (developing inside HepG2 cells) by fluorescence microscopy. We found that mutant EEFs were fewer in number (2.5 ± 0.3 times) and smaller in size (3 ± 1 times) when compared to the wild-type (Figure 2F). When 3,000 mutant sporozoites were injected into rats, there was a delay of one day in the appearance of infected erythrocytes as compared to identical wild-type inoculums. Nevertheless the blood stages developed normally, the mutants produced normal gametocytes, and a new mutant cycle could be established. We tested in vitro whether exogenous expression of CS could complement the CS pexel mutant growth defect. Figure 2G shows that CS complements the growth defect in a dose dependent manner. Using 0.9 μg plasmid

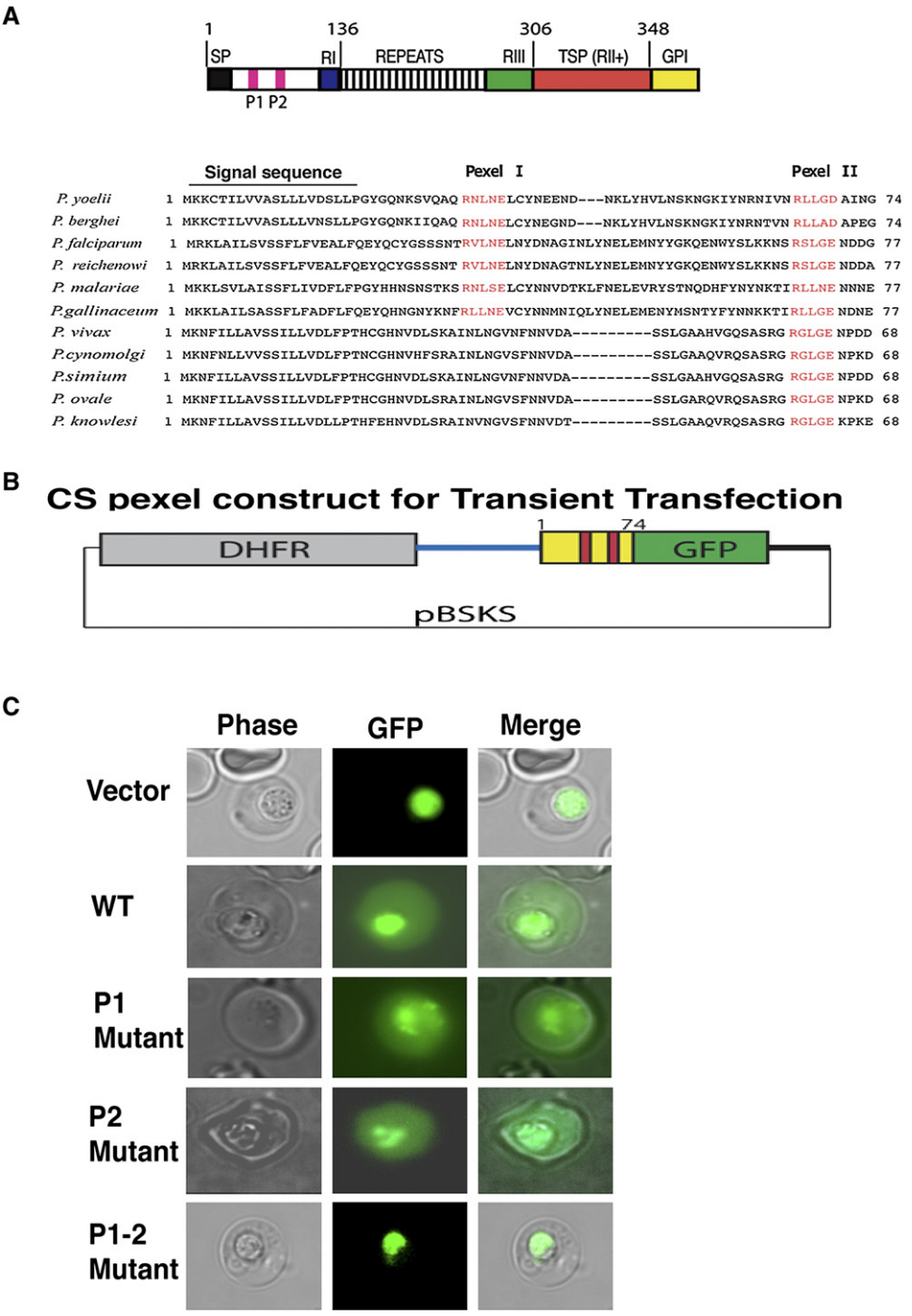

Figure 1. CS Has Functional Pexel/VTS Motifs

(A) Top: schematic representation of the *P. yoelii* CS gene. Two pexel motifs in the N terminus are indicated by P1 and P2. SP, signal peptide; RI, RII+, RIII are conserved regions of CS; GPI, glycosylphosphatidyl inositol attachment site. Bottom: clustal alignment of the N-terminal sequences from various *Plasmodium* species. Two pexel motifs are evident from the alignment. Motif 1 is absent in P. *vivax* and from related monkey malaria species.

(B) The plasmid construct used for transient transfection of erythrocytes containing *P. berghei* schizonts. The bold blue line represents the EF-1α promoter while the black bold line indicates the 3′ UTR from the *P. berghei* DHFR-TS. The CS sequence is depicted in yellow with the two pexel motifs shown in red, and is fused in frame with GFP depicted in green.

(C) Fluorescence and phase images of *P. berghei* in red blood cells transfected with episomal constructs indicated on the left hand side. The images show that both pexel (P) motifs function independently. Mutation of both pexel motifs simultaneously (P1-2) abolishes translocation of CS into the cytoplasm.

per 200,000 HepG2 cells, we achieved a 6-fold increase in the CS pexel mutant parasite growth.

CS Localizes to the Host Nucleus at Early Stages of Hepatocyte Infection

To study the kinetics of the entry of CS into the cytoplasm of the HepG2 cells, we performed a time-course analysis of infection with *P. berghei*. We found that, at early time points, the EEFs surrounded the hepatocyte nucleus and, unexpectedly, that CS was present not only in the cytoplasm but also inside the nucleus of the HepG2 (Figure 3A and Figure S2). Identical results were obtained with *P. yoelii* (not shown). The intra-nuclear CS signal peaked at two hours after sporozoite invasion of hepatocytes, diminished gradually afterwards, and was undetectable after eight hours (Figure 3B), suggesting that CS was actively exported out of nucleus. Indeed, following treatment of the infected hepatocytes with leptomycin B, a specific inhibitor of the Crm1 pathway which is involved in nuclear export of proteins and certain classes of RNAs (Fornerod et al., 1997), CS remained much longer inside the nucleus (Figure 3B and 3C). The infected cells do not show a very strong accumulation of CS in the host nucleus. To avoid the complications of signal overflow arising from the very large quantities of CS associated with parasite, and to provide additional proof that CS localizes to the host nucleus, we expressed ΔCS transiently in HeLa cells. Figure S3 shows that CS is present inside nucleus and in the cytoplasm.

The NLS of CS Is Functional

Deletions in the CS gene combined with inducible translocation trap (ITT) methodology (Hoshino et al., 2004, 2006) was used to localize the CS NLS. Various segments of a *P. yoelii* "humanized" CS (codon optimized) gene were cloned in frame in the vector pLGV, and nuclear import in the reporter cell was monitored as described by Hoshino et al. (2004). As negative and positive controls, we used the empty vector and the NLS of SV40 T-antigen, respectively. A typical flow cytometric analysis result using the above system is shown in Figure 3E. The deletion mapping analysis (Figures 3D and 3F) localized a NLS to the sequence VRVRKRKNV and indicates that there is only one NLS in CS (see constructs 10, 11 and 12 in Figure 3G). The results of the flow cytometric analysis of the various constructs are also shown in Figure 3G.

The NLS function of CS was further validated by transfecting HeLa cells, with plasmids expressing aldolase, a cytoplasmic protein, either alone or fused to the NLS of CS. Only the aldolase fusion protein accumulated into the HeLa cell nucleus (Figure 4A panels a, b). Using the classical nuclear import assay with digitonin-permeabilized HeLa cells (Adam et al., 1992), we documented the energy-dependent nuclear import of rhodamine-labeled BSA coupled to a synthetic peptide encoding the CS NLS (Figure 4B, panel f). The rhodamine-labeled BSA control showed no nuclear accumulation under the same conditions (Figure 4B, panel e). The transport of CS NLS coupled to BSA was competed with molar excess of the CS NLS peptide (Figure 4B, panel g) but not with an unrelated control peptide derived from the WASP protein (data not shown). In addition, nuclear import of rhodamine-labeled CS-NLS was abolished in the presence of an inhibitor of nuclear transport, wheat germ agglutinin (WGA), and considerably reduced at low temperature (data not shown).

The importin α3/β1 Pathway Mediates Nuclear Import of CS

To identify the importin(s) that CS uses to enter the nucleus, we performed in vitro pull-down assays using various recombinant proteins of the importin α family, and in vitro transcribed and translated full-length CS or ΔCS (CS38-328). We reasoned that CS is processed at the N-terminal (Coppi et al., 2005), and that the removal of a portion of the N terminus might influence the exposure of the NLS. However, we found that both full length CS and ΔCS interacted strongly with importin α3 and weakly with importins α4 and α6 (Figures 4C and 4D) . Full-length CS also interacted weakly with α1, α5, and α7 (Figure S4) . Furthermore, we have demonstrated the interaction of known substrates with different importin alphas as positive controls (Figure S4). Although the interaction of CS with these importins is likely direct, we cannot exclude the possibility of an adaptor molecule since the experiments were performed in the presence of reticulocyte lysate.

The binding of CS to importin α3 was abolished after deletion of the nine amino acid residues that encode the NLS. Thus, similar to various regulatory molecules like NFκB (Fagerlund et al., 2005), STAT3 (signal transducer and activator of transcription-3) (Liu et al., 2005) and RCC1 (regulator of chromosome condensation) (Talcott and Moore, 2000), CS is imported into the nucleus preferentially via the importin α3/β1 pathway. Pull-down assays were also used to identify the critical residues in the CS NLS sequence 1-VRVRKRKNV-9 that interact with importin α3 . We found that mutation of R2R4R6 to T2T4T6 abolishes the binding activity of CS to importin α3 (Figure 4D), which is characteristic of this type of NLS (Lange et al., 2007).

CS Enhances EEF Growth in an NLS-Dependent Manner

The striking inhibition of the EEF development in the CS pexel/VTS mutants suggests that the entry of CS into the cytoplasm and/or in the nucleus of hepatocytes enhances EEF growth. As a direct approach to study this question we transiently transfected Hepa 1-6 cells with plasmids expressing *P. yoelii* CS, ΔCS, or ΔCS-ΔNLS. Twenty-four hours posttransfection, hepatocytes were infected with *P. yoelii* sporozoites, and 42 hr postinfection, we measured parasite 18S rRNA copy number by real-time RT-PCR. We found a significant increase in the 18S rRNA copy number in Hepa 1-6 cells transfected with ΔCS as compared to control cells transfected with either full-length CS or empty vector (Figure 5A). These differences are not due to a difference in expression levels (Figure 5A

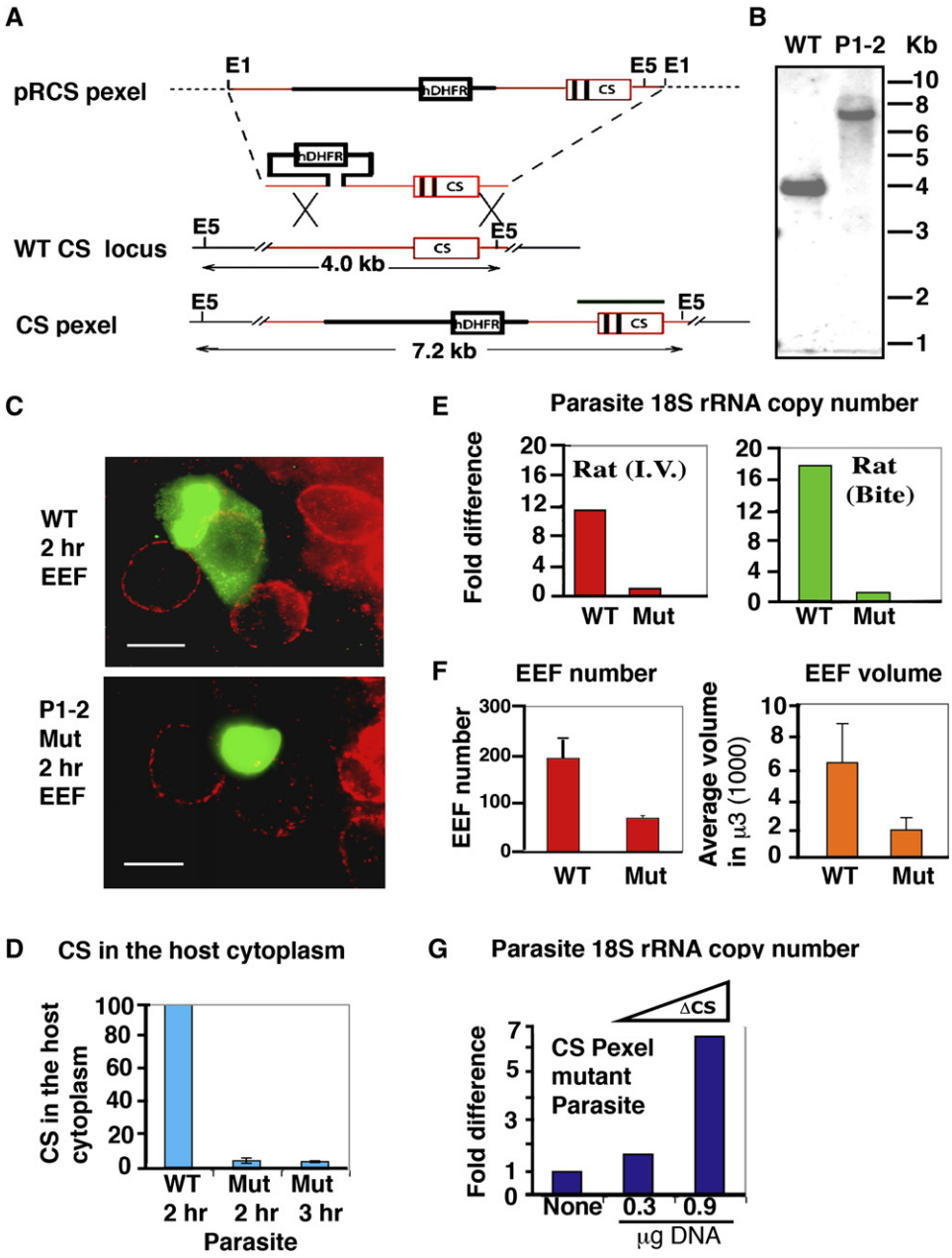

Figure 2. Phenotype of *P. berghei* CS Pexel/VTS Mutants

(A) Schematic of the double crossover strategy used to generate pexel 1-2 double parasite mutants. The *Eco*R V digestion of the genomic DNA from the mutant is predicted to yield a 7.2 kb fragment.

(B) Southern blot analysis of genomic DNA from the wild-type and the CS pexel 1-2 mutant parasites. Expected bands are visible at 4.0 and 7.2 kb for wild-type and mutant, respectively.

(C) The presence of pexel/VTS is required for CS export to the cytoplasm of hepatocyte. Wild-type 2 hr old EEFs export large amounts of CS into the hepatocyte cytoplasm while mutant parasites do not. Please note the presence of CS in both wild-type and mutant EEFs. Scale bar represents 30 μm.

(D) Graph shows the percentage of CS positive cytoplasm in wild-type and CS pexel mutants infecting HepG2 cells. While 100% of HepG2 cells infected with wild-type parasites show cytoplasmic staining, pexel mutants show < 10% cytoplasmic staining at 2 hr and 3 hr time points, respectively. Data represents average and SD of two independent experiments. WT, wild-type; Mut, CS pexel mutant.

(E) In vivo growth of the CS pexel/VTS mutant EEFs as compared to wild-type controls. Infections were performed by intravenous injections and bite. We found a 14 ± 3 fold reduction in mutant EEF growth as measured by parasite 18S rRNA copy numbers. Data shown are from one of three experiments with similar results. Each bar represents average of four animals per group.

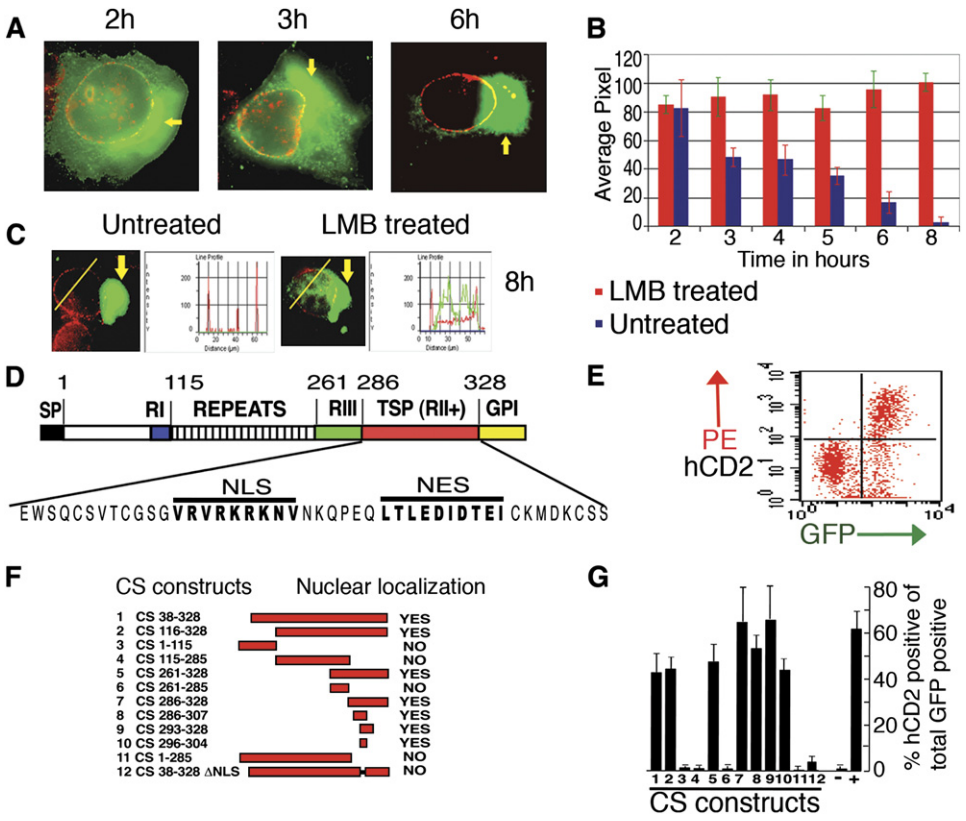

Figure 3. CS Is Imported into the Host Nucleus

(A) The parasite associated (arrow, yellow) and free CS is stained in green using the monoclonal antibody 3D11 and 2° Ab-Alexa 488. The nucleus of HepG2 cells is stained in red with anti-Nup358 antibodies and 2° Ab-Alexa 594. Since the nuclear rim punctate staining was labeled in red (Nup358), it became yellow after merging with green (CS). A total of 25 optical sections were taken and de-convolution was performed using the Auto Visualize, Auto DeBlur v 9.3 program. The pictures are representative of equatorial sections of the host nucleus.

(B) Graph shows pixel intensity in the leptomycin B-treated and untreated cells at different time points. Each data point is the average of two independent experiments with similar results (n = 30) ± SD. Green pixels between the two large red peaks (nuclear limits) were used to calculate the nuclear intensity of CS.

(C) Representative figure of the eight hours time point showing cells and pixel intensity along the line. Pixel intensity was measured using the Image Pro Plus program.

(D) Schematic view of *P. yoelii* CS protein showing the location of the nuclear localization signal (NLS) and the putative nuclear export signal (NES). The other CS regions are also depicted in Figure 1A.

(E) Representative flow cytometric analysis using the ITT system. The upper right quarter represents a CS protein with functional NLS.

(F) CS fragments analyzed in this study. On the right side we state whether the fragments enter the nucleus. Please note that in all the constructs made in pLGV vector, the amino acid number one represents the first amino acid after the signal sequence as marked in Figure 3D.

(G) Quantitation of CS constructs entry into the nucleus of BL2 cells. Graph shows the expression of the reporter gene human CD2 (hCD2) in a mouse cell line (BL2) as percentage of total cells expressing GFP. Each data point shows mean and standard deviation of three independent experiments.

inset). Absence of NLS (ΔCS-ΔNLS) abolished the observed growth with ΔCS indicating that the NLS has a role in the observed enhancement of EEF development. Addition of SRY (sex-determining region on the Y chromosome) cNLS (RPRRKAK) (Sudbeck and Scherer, 1997) to ΔCS-ΔNLS restored CS nuclear import (Figure S5) and CS mediated growth enhancement (Figure 5B). We also counted the EEF numbers in Hepa 1-6 cells transfected with ΔCS (131 ± 11) or vector alone (126 ± 5) at 44 hr post-infection. There was no significant differences between

(F) Graphs show that mutant parasites are fewer in number and are smaller in size as compared to the wild-type. Results are from one of two experiments with similar results. Data represents average of triplicates and SD. Parasite numbers and volume were measured by immunofluorescence microscopy and processed using the Image Pro Plus program (Media cybernetics, USA). WT, wild-type; Mut, CS pexel mutant.

(G) Complementation of CS pexel mutant parasite by ectopically expressed wild-type ΔCS. HepG2 cells were transfected with 0.3 or 0.9 μg of ΔCS-pLGV construct using Lipofectamine 2000 at 1:4 ratio. Twenty-four hours later, CS pexel mutant sporozoites (1000) were allowed to invade. Forty-eight hours post invasion, parasite 18S rRNA copy numbers were measured. Presented is fold increase based on average values of two experiments, each performed in triplicate.

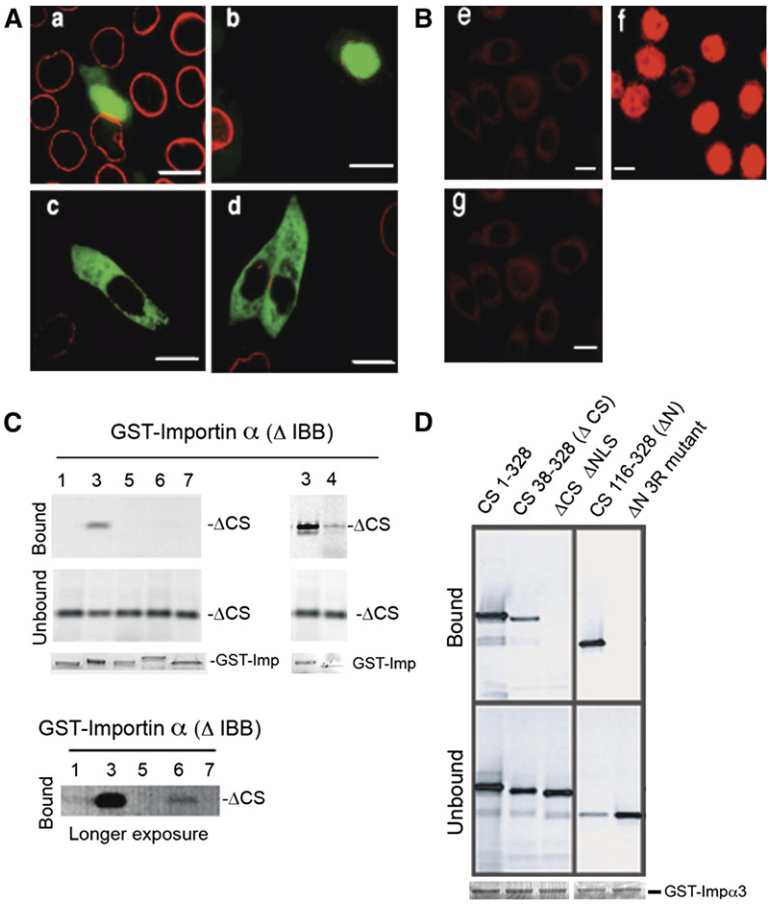

Figure 4. CS NLS Binds Primarily to Importinα3

(A) Nuclear localization of the CS-NLS-aldolase fusion protein. HeLa cells were transfected with plasmids encoding the NLS of CS fused with aldolase of *P. falciparum* (a, b) or with aldolase alone (c, d). Aldolase is stained in green and nuclear membrane is stained in red with anti-Nup358 antibodies. Scale bar represents 30 μm.

(B) In vitro import assay in digitonin-permeabilized HeLa cells. The BSA-rhodamine (e) or CS-NLS-BSA-rhodamine (f) was incubated with cells in the presence of ATP. Nuclear import of CS-NLS-BSA-rhodamine was competed with CS NLS peptide (g). Scale bar represents 30 μm.

(C) ΔCS preferentially interacts with importin α3. In vitro binding assays were performed with immobilized GST-importins α 1, 3, 4, 5, 6, and 7 with deleted importin beta binding domain (ΔIBB) and in vitro transcribed and translated ^{35}S-ΔCS. Bound and unbound fractions were analyzed by SDS-PAGE followed by autoradiography. The amount of GST- importin alphas used in each assay is shown at the bottom panel by Coomassie staining (GST-Imp).

(D) Deletion of the CS NLS (ΔNLS) or mutation of three arginine residues (3R) abolished the interaction of CS with importin α3. In vitro pull-down assays using immobilized GST- importin α3 (with ΔIBB) and in vitro transcribed and translated wild-type CS or mutants of CS were performed as in (C). Coomassie stained importin α3 is shown at the bottom panels.

these values (p value > 0.5), indicating that ΔCS enhances development of the EEFs rather than sporozoite invasion. These results were confirmed by additional experiments in which, the development of EEFs was measured by copy numbers of the merozoite surface protein 1 (MSP1) whose expression starts prior to schizogony, and reaches a maximum toward the end of EEFs development (Figure S6).

CS Inhibits Nuclear Translocation of Transcription Factor NFκB

NFκB binds to importins α3 and α4. Since CS also binds to importin α3 and to a less extent to importin α4, we entertained the possibility that EEFs may interfere with the NFκB entry into the nucleus. To approach this question experimentally, a monolayer of HepG2 cells was infected with *P. berghei* sporozoites and treated with the proinflammatory cytokine hTNFα to induce NFκB nuclear translocation. Cells were then stained with antibodies to NFκB p50 (Figure 6A). When compared to noninfected cells in the same monolayer, there was a profound inhibition of the intensity of the NFκB p50 staining in infected cells (75 ± 20% decrease, range 50%–90%, n = 3 and 50 cells counted per experiment). Similar results were obtained with early (5 hr) and mature (48 hr) EEFs.

To determine whether the inhibition of NFκB nuclear import by EEFs was mediated by CS, we generated HeLa cells expressing ΔCS under the control of the Tet promoter (Gossen and Bujard, 1992). HeLa cells were treated with doxycycline followed by hTNFα. The nuclear fractions were separated on SDS-PAGE and probed with antibodies to NFκB p50. We found a significant reduction (2/3) of nuclear NFκB p50 in ΔCS containing (+ doxycycline) cells (Figure 6B). To investigate whether ΔCS inhibits active NFκB (p50/p65), we performed a gel shift assay. Nuclear extract from TNFα induced HeLa or HeLa-ΔCS was incubated with biotin-labeled NFκB target duplex oligos and bound complexes were separated on a native gel. Figure 6C shows that CS inhibits 75 ± 5% of NFκB entry into the nucleus.

The presence of CS in the cytoplasm of HeLa cells did not affect the phosphorylation and degradation of IκB (Figure 6D), indicating that the steps preceding the NFκB release from its inhibitory complex were not affected. A definite demonstration of NFκB inhibition by CS was achieved by the whole genome microarray analysis (U133 chip) using HeLa cells expressing ΔCS and comparing it with control HeLa cells not expressing ΔCS. We found that at least forty NFκB responsive genes were downregulated in the presence of ΔCS (Table S1 and Figure 6E). Of

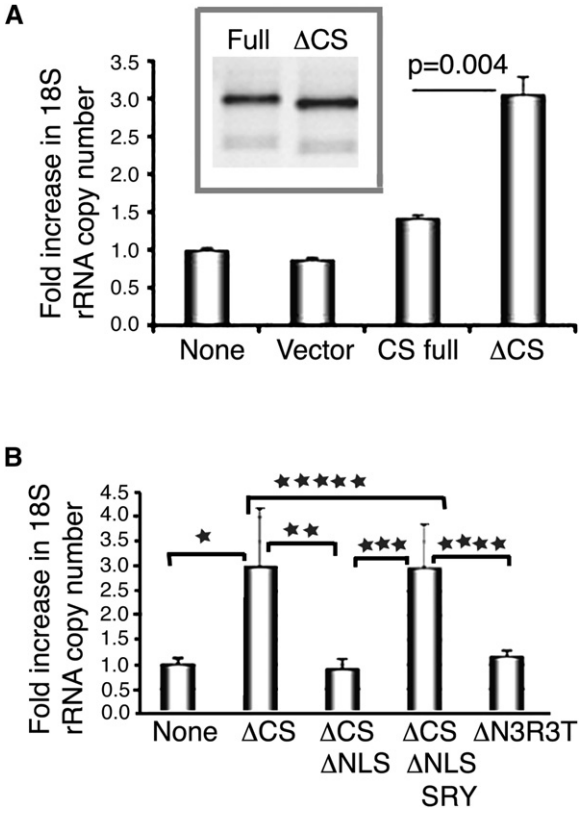

Figure 5. CS NLS-Dependent Enhancement of Parasite Growth

(A) The graph shows the fold increase in *P. yoelii* 18S rRNA copy numbers of parasite growing inside Hepa1-6 hepatocytes transfected with the indicated plasmids. Values shown are mean of triplicate with SD. Results are from one of three independent experiments with similar values. CS constructs are those shown in Figure 3F. The p value between the two groups was calculated by two tailed, Students t test method using normalized 18S rRNA copy numbers. Inset shows the expression levels as determined by Western blot analysis. There is no difference in the expression levels between the two constructs.

(B) Enhancement of growth is NLS dependent. Copy number of parasite growing inside Hepa1-6 hepatocytes transfected with the indicated DNA inserts in the pLGV vector. Deletion of the CS NLS or mutations in the three arginine-residues of the NLS abolished ΔCS-mediated growth enhancement. In the case of the ΔCS with deleted NLS, the growth enhancement was restored by the addition of a heterologous NLS from the SRY protein. Values shown are mean of triplicates with standard deviations. Results are representative data from one of two independent experiments. p values were calculated by one-way ANOVA test. p*, **, ***, **** < 0.05; ***** > 0.05.

all the genes that were at least four fold upregulated by TNFα treatment, 85% of them were significantly downregulated (>2 fold, $p < 0.05$) in presence of ΔCS. Microarray data also confirmed our observation that upstream signaling is not altered in the presence of ΔCS. The data discussed in this publication have been deposited in NCBIs Gene Expression Omnibus (GEO, http://www.ncbi.nlm.nih.gov/geo/) and are accessible through GEO Series accession number GSE8784.

Next, we infected HepG2 monolayers with the CS pexel mutant or wild-type parasites, treated the monolayers with TNFα, and compared the intensities of NFκB p65 staining in the nuclei of infected and noninfected hepatocytes 48 hr postinfection (Figure 7). While the wild-type parasites inhibited nuclear translocation of NFκB by approximately 85%, the level of inhibition in the mutants was only 20 ± 10%, ranging from 5%–30% (n = 3 and 50 cells counted per experiment).

Previously, it was reported that, at concentration of 0.1–0.2 mM, CS inhibits protein synthesis (Frevert et al., 1998) in vitro. However, no inhibition was noted in HepG2 cells containing parasites using radio-autography (Frevert et al., 1998). We used a different approach to study this possibility. We cotransfected HeLa cells with plasmids expressing vector alone or CS in a luciferase reporter gene assay. At 24–48 hr posttransfection, we did not observe any differences in protein synthesis (Figure S7).

DISCUSSION

Plasmodium blood stages develop inside a PV and export to the erythrocyte cytoplasm a group of soluble and membrane virulence proteins that promote infection and parasite survival. These proteins use a signal sequence to enter the secretory pathway, and many bear a conserved pentameric motif required for the passage though the PV membrane. This motif, named pexel/VTS, permitted the prediction in silico of the *Plasmodium* "exportome." The precise mechanisms that drive pexel/VTS soluble and trans-membrane proteins through the PV have not been elucidated.

EEFs also grow inside a PV, and CS is one of the EEF surface proteins that is exported to the hepatocyte cytoplasm. We show here that the traversal of CS through the PV membrane is mediated by pexel/VTS motifs present at the N-terminal region of CS. We generated a *P. berghei* mutant parasite, whose CS contained inactive pexel/VTS motifs. The mutant and wild-type salivary gland sporozoites were equally infective for HepG2 cells. As predicted by the results of the transfection experiment, CS did not enter the cytoplasm of most hepatocytes infected with mutants. Mechanistically, it is not known how a pexel/VTS motif guides soluble proteins through the PV membrane. One possibility is that it is a sorting signal that binds to a specialized translocator that move the complex through specific PV pores. The nature of the putative translocator is unknown, but if it exists, it should be shared between EEFs and blood stages. The interaction of CS with the translocator probably take place in the lumen of the PV prior to export (Marti et al., 2005).

In addition to the N-terminus pexel/VTS motifs, CS has a functional NLS motif encompassing the conserved, positively charged, C terminus region II-plus. A pool of CS enters the hepatocyte nucleus where it is detected by immunofluorescence from 1–4 hr after sporozoite invasion. To reveal the role of the CS translocation from the EEFs into the cytoplasm and nucleus of hepatocytes, we

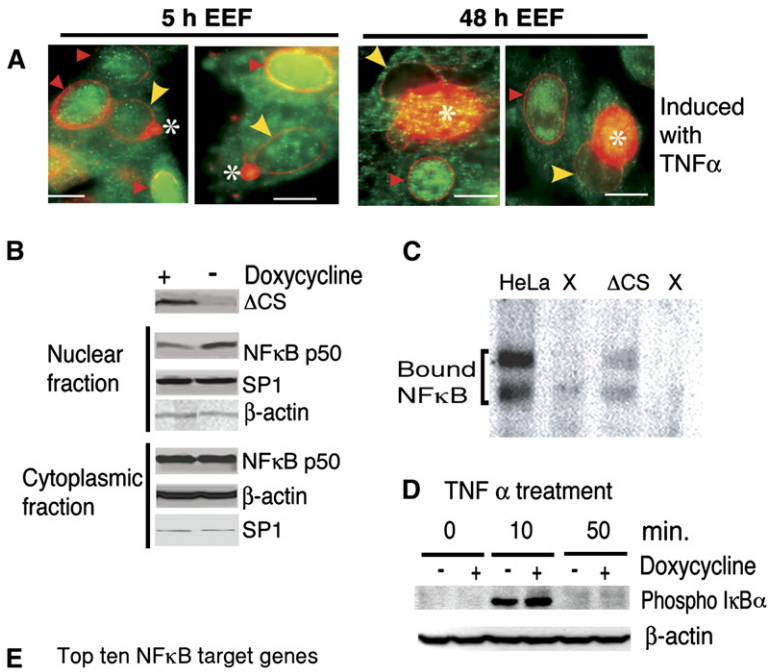

E Top ten NFκB target genes down regulated by ΔCS

Probeset	Gene	Description	Fold down
206524_at	T box	T box containing (Brachyury homologue)	77.03
205476_at	CCL20	MIP3 α	64.96
210587_at	INHBE	Inhibin β E	50.45
201313_at	ENO2	Enolase 2 γ	33.53
205127_at	PTGS1	Prostaglandin endoperoxide synthase 1	22.23
204417_at	GALC	Ceramide glycosyl transferase	10.16
215446_s_at	LOX	Receptor for oxidized low density lipoprotein	8.27
202627_s_at	SERPINE1	Serpin peptidase inhibitor, clade E member 1	7.66
204719_at	ABCA8	ATP-binding cassette, sub-family A member 8	7.58
203868_s_at	VCAM1	Vascular cell adhesion molecule	6.36

Figure 6. CS Interferes with Nuclear Translocation of NFκB

(A) Nuclear NFκB p50 staining in infected and noninfected HepG2 cells. Two or forty five hours old EEFs were treated with 20 ng/ml hTNFα for three hours, and stained with monoclonal antibody to NFκB p50 (2°Ab green), rabbit antibodies to Nup358 and *P. berghei* aldolase antibody (2°Ab red). EEFs are marked with stars. There is a marked decrease in NFκB p50 in the infected cells (arrow head yellow) as compared to the noninfected cells (arrow head red). Scale bar represents 30 μm.

(B) Levels of nuclear NFκB p50 in HeLa cells expressing or not expressing ΔCS following induction by TNFα. The levels of NFκB p50 were measured by Western blot. In the presence of ΔCS, there was a reduction of NFκB p50 in the nuclear fraction while the levels of NFκB in the cytoplasm were unaltered. SP1 and β-actin were used as nuclear and cytoplasmic loading controls, respectively.

(C) Gel shift assay shows that ΔCS inhibits activated NFκB nuclear translocation. TNFα activated nuclear extract (50 μg) and biotin-labeled NFκB duplex oligos were used. X represents empty lane.

(D) Phosphorylation and degradation of IκBα in the HeLa cells that, express, or do not express ΔCS. Expression of ΔCS does not alter phosphorylation and degradation of IκBα.

(E) List of the ten most downregulated NFκB target genes due to expression of ΔCS. Data is derived from a whole genome microarray data (accession number GSE8784) of ΔCS expressing HeLa cells compared to nonexpressing cells.

analyzed the phenotype of the pexel/VTS mutants of CS. The mutant EEFs were much smaller in size and contained 14× less parasite rRNAs than wild-type. Fewer mutants were detected in the monolayer of infected hepatocytes, suggesting that some mutants did not grow or were too small. The observation that exported CS promotes EEF development was further supported by additional experiments which showed that the EEFs growth is significantly enhanced in hepatocyte cell lines transfected with plasmids expressing ΔCS, but not full length CS (Figure 5A). Ectopically expressed ΔCS complemented CS pexel mutant growth defect in a dose-dependent manner Figure 2E).

We cannot exclude the possibility that EEF growth is contingent on the entry of CS into the hepatocyte nucleus. However, we favor the idea that the site of CS activity is the cytoplasm, and that the NLS of CS competes successfully with other importins α3/β1 cargos that are noxious to the parasite development. Since EEFs grow embracing the hepatocytes nucleus, the concentration of CS will be larger in the perinuclear region where it should displace transcription factors that bind to importins α3.

It is likely that the growth enhancing mechanism is multifactorial and involves multiple metabolic/signaling pathways. This hypothesis is strongly supported by the microarray data.The list of transcription factors that bind importin α3 is far from complete, but includes NFκB (Fagerlund et al., 2005), STAT3 (Liu et al., 2005) and RCC1 (Talcott and Moore, 2000). NFκB controls the expression of multiple genes involved in inflammation (Aggarwal, 2004). STAT3 activates a wide variety of genes that control cell proliferation and survival, and in its absence, acute phase response associated with infections is inhibited (Alonzi et al., 2001). IL-6 inhibits EEF growth (Pied et al., 1992) and IL-6 secretion is downregulated by the parasite (Pied et al., 1992). RCC1 regulates the distribution of the small Ran GTPase that provide directionality to nuclear transport between the nucleus and the cytoplasm (Weis, 2003). Interference with RCC1 by the parasite may disrupt nucleocytoplasmic trafficking.

We observed the effect of EEFs and CS on the traffic of NFκB into the hepatocyte nucleus. After treating a monolayer of infected HepG2 cells with TNFα to activate the NFκB pathway, the entry of NFκB into the hepatocyte

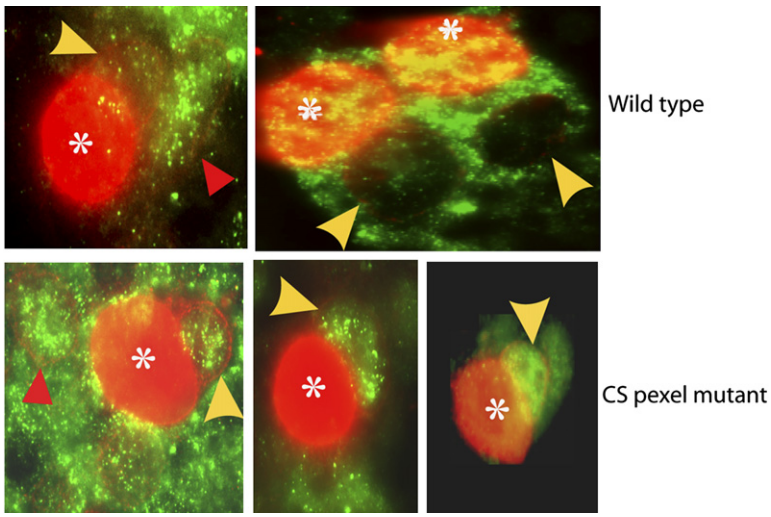

Figure 7. Nuclear Import Inhibition of NFκB Is Partially Reverted in CS Pexel Mutant EEFs

Nuclear NFκB p65 staining in wild-type and CS-pexel mutant infected HepG2 cells. Sixty-eight hour old EEFs were treated with 40 ng/ml hTNFα for 3 hr and stained with monoclonal antibody to NFκB p65 (2°Ab green), rabbit antibodies to Nup358, and *P. berghei* aldolase antibody (2°Ab red). EEFs are marked with *. In the case of wild-type parasite infected HepG2 cells, the nucleus of infected cell (arrowhead yellow) but not of the uninfected cell (arrowhead red), show reduced staining of NFκB p65. Infected and the neighboring uninfected HepG2 cells were identified by optical sectioning. At bottom, CS pexel/VTS mutant infected cell (arrowhead yellow) shows a partial reversal of NFκB nuclear translocation. Nucleus of uninfected cell is marked with a arrowhead (red). While the wild-type parasites inhibited nuclear translocation of NFκB p65 ~85%, the level of inhibition in the mutants was only 20 ± 10%.

nucleus was strongly inhibited in the presence of EEFs as compared to noninfected cells (Figure 6A). The inhibition is likely to be at least in part CS-mediated since it is also observed in HeLa cells expressing ΔCS (Figures 6B and 6C).

Whole genome microarray data (accession number GSE8784) from ΔCS expressing HeLa cells revealed that at least 40 NFκB targets were more than two-fold downregulated and among them several NFκB targets were more than ten-fold downregulated (Figure 6E). Inflammation related genes CCL20 (also known as MIP3 α) and PTGS1 transcripts were sixty-five and twenty-two fold downregulated, respectively ($p < 0.05$). Inhibin β E (also known as Activin β E) belongs to TGF β family, and induces apoptosis in HepG2 cells (Chabicovsky et al., 2003). Inhibin β E was fifty-fold downregulated. Folstatins antagonize inhibin action and we found Folstatin-4 was 4-fold upregulated (Table S2). The GALC (Galactosyl-ceramidase) transcript was downregulated 10-fold (Figure 6E). Glycolipid alpha-Galcer is a known agonist of NKT cells and bind to CD1d receptor expressed on NKT cells (Taniguchi et al., 2003). Recently it was shown that NFκB also regulates the expression of micro RNA miR-146 a/b (Taganov et al., 2006). Thus, inhibition of NFκB may indirectly expand the number of affected genes. Our findings thus provide an explanation for the puzzling observation that EEFs grow for many days in the liver without provoking an inflammatory response (Short et al., 1954).

Microarray data also revealed that CS has targets besides NFκB. Overall ~1,000 genes were downregulated and ~100 genes were upregulated 2 fold or more ($p < 0.05$, t test, Table S2). These genes govern diverse biological functions such as metabolite transport, cell cycle, immune responses, cell growth, cell attachment, apoptosis and hypoxia and the overall effect is to enhance EEF growth. It remains to be established how CS modulates the non-NFκB target genes.

We conclude that EEFs and the erythrocytic stages of malaria use the same strategies to ensure parasite development in the mammalian hosts. Both stages of *Plasmodium* reside inside PVs and use the pexel/VTS motif to export virulent proteins into the cytoplasm of the respective host cells in order to promote survival and development of the parasite. Although the mechanisms differ, many micro organisms modify the host environment to their benefit. Competition with importins has been noted in few instances. In the hepatitis C virus, the nonstructural protein 5A (NS5A) appears to compete with substrates that naturally interact with importin β3, but the role of NS5A in viral survival and replication is not known (Chung et al., 2000). In the case of Ebola Virus, VP24 protein binds to importin α1 and block the nuclear translocation of phosphorylated STAT1 (Reid et al., 2006). Similar to CS, VP24 is also found in the perinuclear region.

The intracellular apicomplexan parasite, *Toxoplasma*, that like *Plasmodium*, develops inside a PV, blocks the translocation of NFκB into the host cell nucleus during early stages of infection (Denkers, 2003; Shapira et al., 2004). Toxoplasma proteins do not bear pexel/VTS motifs, nevertheless the parasite modulates host cell transcription by injecting polymorphic protein kinases (ROP16 and ROP18) and probably other proteins into the host cell cytoplasm (Saeij et al., 2006, 2007; Taylor et al., 2006). Toxoplasma also injects into the host cell cytoplasm a parasite phosphatase 2C. The enzyme contains a NLS and enters the nucleus. Disruption of the gene encoding the phosphatase leads to a mild parasite growth defect (Gilbert et al., 2006).

CS is also a dominant T cell antigen (Kumar et al., 2006). Thus, the passage of EEF proteins into the cytoplasm of hepatocytes increases the risk of recognition of infected cell by the host's immune system. Nevertheless the CS export from the PV is also central for parasite development.

This is an example of the delicate balance that must exist to permit the simultaneous parasite and host survival. The identification of the secretome of EEFs will most likely provide new targets for drug and vaccine development and a better understanding of EEF biology. Computational methods indicate that less than twenty five proteins of sporozoites contain the pexel motif (Marti et al., 2004) and may enter the hepatocyte cytoplasm. Large strides can probably be made, by analyzing the function of other members of the EEF exportome.

CS plays a central role in several stages of the parasite life cycle. It is essential for sporozoite development in the oocysts (Menard et al., 1997), for the exit of sporozoites from oocysts (Wang et al., 2005), for their entry into the salivary gland of the mosquitoes (Myung et al., 2004), for the attachment and invasion of hepatocytes (Cerami et al., 1992) and as shown here for EEF development. Thus CS is a master regulator of *Plasmodium* pre-erythrocytic stages development.

EXPERIMENTAL PROCEDURES

Transfections

Mutant parasites were generated by the double crossover replacement method (Menard and Janse, 1997). Cloning and Southern blot analysis were performed as in Wang et al., 2005.

In Vivo and In Vitro Growth Assay

C57BL/6 mice or S/D rats were injected intravenously with 40,000 sporozoites. For infection by bite, ten infected mosquitoes/young rat were used for 10 min. Forty-eight hours postinfection RNA was extracted from the liver. For in vitro growth measurement, Hepa1-6 cells, grown in 24-well plates, were transfected with 0.8 μg of the indicated plasmids. Twenty-four hours post transfection, 30,000 *P. yoelii* sporozoites were added, and RNA was extracted forty-two hours post infection. Real-time PCRs to measure parasite rRNA (Bruna-Romero et al., 2001) were performed with 18S rRNA primers and copy number normalized by host GAPDH copy numbers.

EEF Number and Size Measurements

Hepa1-6 or HepG2 cells were seeded on coverslips and *P. yoelii* or *P. bergehi* sporozoites were used for infection. Coverslips were fixed, permeabilized, and subjected to immunoflourescence staining with anti-HSP70 antibody (Tsuji et al., 1994). The number of EEFs was counted in a fluorescence microscope. To measure EEF size, mature EEFs were imaged using a fluorescence microscope at 100× magnification. Radius and area measurements were done using Image Pro Plus program (Media Cybernetics, USA).

Gliding Motility and Double Staining of Sporozoite

Gliding assay was performed as described by Stewart (Stewart and Vanderberg, 1991) and parasite double staining was previously described by Renia (Renia et al., 1988).

CS Distribution in the Hepatocytes

HepG2 cells were seeded onto glass coverslips one day prior to invasion with *P. berghei* sporozoites. Cells were fixed, permeabilized and subjected to immunoflourescence staining with anti *P. berghei*-CS (3D11) and anti-Nup358 antibodies (Wu et al., 1995). To monitor the inhibition of export, leptomycin B was added at 6 ng/ml 1 hr after addition of sporozoites. Images were captured on a Nikon Eclipse 800 microscope at 100x magnification and deconvolution was performed iteratively using the 2-D Blind method.

ITT Methodology Using CS Constructs

Deletions or point mutation of CS were made in the pLGV vector (Hoshino et al., 2004). *P. yoelii* CS fragments (codon sequence humanized) were introduced in the *Hind* III- *Not* I sites of the pLGV vector. Each pLGV derived plasmid was cotransfected with equal amounts of ectopic helper vector (psi2) into 293T cells, and incubated for forty-eight hours to obtain the replication-deficient retroviruses in the culture supernatant. Mouse hematopoietic Ba/F3-derived BL2 cell line with the human CD2 (hCD2) reporter gene integrated in the genome under control of LexA operator (8x-LexA) were infected with virus encoding various CS sequences and incubated for 48 hr to allow expression of the reporter gene (hCD2). Two days postinfection, BL2 cells were stained with anti-hCD2 antibody and with a secondary antibody coupled to phyco-erythrin (PE). Stained BL2 cells were analyzed for GFP and hCD2 with FACS Calibur cytometer (BD Biosciences).

Aldolase-NLS Fusion Proteins

The *P. falciparum* aldolase gene alone or fused to CS NLS were cloned into pCDNA3.1A (Invitrogen) at *Hind* III-*Not* I sites. A Kozak sequence was also inserted at the *Hind* III site. HeLa cells were transfected with these plasmids and, after 24 hr, cells were fixed, permeabilized, and stained with antibodies against the *P. falciparum* aldolase, and with anti- Nup358 antibodies. The antibodies to the parasite aldolase do not react with mammalian aldolases (C.A.B., unpublished data).

Import and In Vitro Binding Assays

Nuclear import assay was performed (Adam et al., 1992) using the rhodamine-labeled BSA coupled to CS-NLS. Expression of importins, purification, and in vitro binding assays were carried out as previously described (Fontoura et al., 2000; Faria et al., 2005) using 10 μl in vitro translated CS proteins and 1 μg importins. Bound and unbound fractions were separated on SDS-PAGE and analyzed by autoradiography.

Immunofluorescence and Microscopy for NFκB

EEF-containing HepG2 cells were treated with hTNFα (Upstate Cell Signaling) for 3 hr and subjected to immunofluorescence staining with anti-NFκB p50 or p65 monoclonal antibody (Santa Cruz Biotech). Parasites and host nuclear membrane were detected with antibodies to aldolase (Buscaglia et al., 2003) and Nup358 (Wu et al., 1995) respectively. Intranuclear NFκB intensity was measured by the Image pro plus program.

Nuclear NFκB p50 and Phospho-IκBα Measurements in TNFα-Treated Cells

HeLa cell clones expressing ΔCS under the control of the tet promoter were generated using the Retro-Tet-ON™ system (BD Biosciences). The HeLa cell clones were treated with 1 μg/ml doxycycline for 16 hr followed by hTNFα (20 ng/ml) for six hours. Cytoplasmic and nuclear fractions were prepared using NE-PER Kit (Pierce). Equal amounts of cytoplasmic or nuclear fractions were separated on SDS-PAGE, transferred to PVDF membrane, and probed with the NFκB p50 monoclonal antibody followed by ECL reagent (Amersham Biosciences). The membrane was stripped and re-probed with anti-SP1 and anti-β actin (Sigma,). Phosphorylation and degradation of IκBα was analyzed from HeLa-tet-ΔCS cells treated with 1 μg/ml doxycycline for 16 hr followed by hTNFα (20 ng/ml) for 0, 10, and 50 min. Fifty micrograms of total cell lysate was then transferred to a PVDF membrane and probed with anti-phospho IκBα antibody.

Gel Shift Assay

NFκB target oligos (sense) 5′-AGTTGAGGGGACTTTCCCAGGC-3′ and (anti) 5′-GCCTGGGAAAGTCCCCTCAACT-3′ were biotin labeled using biotin 3′ end DNA labeling kit (Pierce). Oligos were annealed and used directly. The binding mixture (20 μl) containing 1× binding buffer, KCl 50 mM, $MgCl_2$ 5 mM, $ZnCl_2$ 1.5 mM, glycerol 5%, 0.05% NP-40, 50 μg/ml Poly I:C (Lightshift EMSA kit, Pierce), 20 femto-mole annealed oligo, and 50 μg nuclear extract was incubated at 25°C for

30 min. Bound complexes were separated on 5% Native PAGE and visualized using chemiluminescent DNA detection kit (Pierce).

Gene Chip Analysis

To determine the effect on genes regulated by NFκB, HeLa cells bearing the ΔCS construct were first induced with doxycycline for 17 hr and then exposed to TNFα (40ng/ml), RNA samples were collected after 6 hr, labeled, and hybridized to high density Affymetrix arrays (U133).

Supplemental Data

Supplemental Data include Supplemental Experimental Procedures and Results, Supplemental References, seven figures, and two tables and can be found with this article online at http://www.cell.com/cgi/content/full/131/3/492/DC1/.

ACKNOWLEDGMENTS

We thank Dr. David E. Levy (NYU) for helpful discussions and reagents. Thanks are also due to Drs. Nancy C. Reich (Stony Brook University, NY) and Riku Fagerlund (NPHI, Finland) for providing importin α expression constructs, Dr. E. Fodor (Oxford, England) for plasmid NP-pCDNA, M. Michael (University of California, San Diego) for plasmid PK-NLS (hnRNPK) pCDNA, Dr. Photini Sinnis (NYU) for plasmid pWTREP, and Dr. Andy Waters (Leiden University, Netherlands) for plasmid pL0016. We thank Mingyuan Tao (NYU) and Neal Satterly (UTSW) for providing the experimental assistance. We thank Dr. Ruth Nussenzweig for critical reading of the manuscript. This work was supported by grants to V.N. (Dana Foundation), H.F. (NIH-AI 059315), and B.M.A.F. (NIH-GM067159).

Received: January 9, 2007
Revised: May 15, 2007
Accepted: September 4, 2007
Published: November 1, 2007

REFERENCES

Adam, S.A., Sterne-Marr, R., and Gerace, L. (1992). Nuclear protein import using digitonin-permeabilized cells. Methods Enzymol. *219*, 97–110.

Aggarwal, B.B. (2004). Nuclear factor-kappaB: the enemy within. Cancer Cell *6*, 203–208.

Alonzi, T., Maritano, D., Gorgoni, B., Rizzuto, G., Libert, C., and Poli, V. (2001). Essential role of STAT3 in the control of the acute-phase response as revealed by inducible gene inactivation [correction of activation] in the liver. Mol. Cell. Biol. *21*, 1621–1632.

Bruna-Romero, O., Hafalla, J.C., Gonzalez-Aseguinolaza, G., Sano, G., Tsuji, M., and Zavala, F. (2001). Detection of malaria liver-stages in mice infected through the bite of a single Anopheles mosquito using a highly sensitive real-time PCR. Int. J. Parasitol. *31*, 1499–1502.

Buscaglia, C.A., Coppens, I., Hol, W.G., and Nussenzweig, V. (2003). Sites of interaction between aldolase and thrombospondin-related anonymous protein in plasmodium. Mol. Biol. Cell *14*, 4947–4957.

Cerami, C., Frevert, U., Sinnis, P., Takacs, B., Clavijo, P., Santos, M.J., and Nussenzweig, V. (1992). The basolateral domain of the hepatocyte plasma membrane bears receptors for the circumsporozoite protein of Plasmodium falciparum sporozoites. Cell *70*, 1021–1033.

Chabicovsky, M., Herkner, K., and Rossmanith, W. (2003). Overexpression of activin beta(C) or activin beta(E) in the mouse liver inhibits regenerative deoxyribonucleic acid synthesis of hepatic cells. Endocrinology *144*, 3497–3504.

Chung, K.M., Lee, J., Kim, J.E., Song, O.K., Cho, S., Lim, J., Seedorf, M., Hahm, B., and Jang, S.K. (2000). Nonstructural protein 5A of hepatitis C virus inhibits the function of karyopherin beta3. J. Virol. *74*, 5233–5241.

Coppi, A., Pinzon-Ortiz, C., Hutter, C., and Sinnis, P. (2005). The Plasmodium circumsporozoite protein is proteolytically processed during cell invasion. J. Exp. Med. *201*, 27–33.

Denkers, E.Y. (2003). From cells to signaling cascades: manipulation of innate immunity by Toxoplasma gondii. FEMS Immunol. Med. Microbiol. *39*, 193–203.

Desai, S.A., and Rosenberg, R.L. (1997). Pore size of the malaria parasite's nutrient channel. Proc. Natl. Acad. Sci. USA *94*, 2045–2049.

Fagerlund, R., Kinnunen, L., Kohler, M., Julkunen, I., and Melen, K. (2005). NF-{kappa}B is transported into the nucleus by importin {alpha}3 and importin {alpha}4. J. Biol. Chem. *280*, 15942–15951.

Faria, P.A., Chakraborty, P., Levay, A., Barber, G.N., Ezelle, H.J., Enninga, J., Arana, C., van Deursen, J., and Fontoura, B.M. (2005). VSV disrupts the Rae1/mrnp41 mRNA nuclear export pathway. Mol. Cell *17*, 93–102.

Fontoura, B.M., Blobel, G., and Yaseen, N.R. (2000). The nucleoporin Nup98 is a site for GDP/GTP exchange on ran and termination of karyopherin beta 2-mediated nuclear import. J. Biol. Chem. *275*, 31289–31296.

Fornerod, M., Ohno, M., Yoshida, M., and Mattaj, I.W. (1997). CRM1 is an export receptor for leucine-rich nuclear export signals. Cell *90*, 1051–1060.

Frevert, U., Galinski, M.R., Hugel, F.U., Allon, N., Schreier, H., Smulevitch, S., Shakibaei, M., and Clavijo, P. (1998). Malaria circumsporozoite protein inhibits protein synthesis in mammalian cells. EMBO J. *17*, 3816–3826.

Gilbert, L.A., Ravindran, S., Turetzky, J.M., Boothroyd, J.C., and Bradley, P.J. (2006). Toxoplasma gondii targets a protein phosphatase 2C to the nucleus of infected host cells. Eukaryot. Cell *6*, 73–83.

Gossen, M., and Bujard, H. (1992). Tight control of gene expression in mammalian cells by tetracycline-responsive promoters. Proc. Natl. Acad. Sci. USA *89*, 5547–5551.

Hiller, N.L., Bhattacharjee, S., van Ooij, C., Liolios, K., Harrison, T., Lopez-Estrano, C., and Haldar, K. (2004). A host-targeting signal in virulence proteins reveals a secretome in malarial infection. Science *306*, 1934–1937.

Hollingdale, M.R., Leland, P., Leef, J.L., Leef, M.F., and Beaudoin, R.L. (1983). Serological reactivity of in vitro cultured exoerythrocytic stages of Plasmodium berghei in indirect immunofluorescent or immunoperoxidase antibody tests. Am. J. Trop. Med. Hyg. *32*, 24–30.

Hoshino, A., Matsumura, S., Kondo, K., Hirst, J.A., and Fujii, H. (2004). Inducible translocation trap: a system for detecting inducible nuclear translocation. Mol. Cell *15*, 153–159.

Hoshino, A., Saint Fleur, S., and Fujii, H. (2006). Regulation of Stat1 protein expression by phenylalanine 172 in the coiled-coil domain. Biochem. Biophys. Res. Commun. *346*, 1062–1066.

Hugel, F.U., Pradel, G., and Frevert, U. (1996). Release of malaria circumsporozoite protein into the host cell cytoplasm and interaction with ribosomes. Mol. Biochem. Parasitol. *81*, 151–170.

Kumar, K.A., Sano, G., Boscardin, S., Nussenzweig, R.S., Nussenzweig, M.C., Zavala, F., and Nussenzweig, V. (2006). The circumsporozoite protein is an immunodominant protective antigen in irradiated sporozoites. Nature *444*, 937–940.

Lange, A., Mills, R.E., Lange, C.J., Stewart, M., Devine, S.E., and Corbett, A.H. (2007). Classical nuclear localization signals: Definition, function, and interaction with importin alpha. J. Biol. Chem. *282*, 5101–5105.

Liu, L., McBride, K.M., and Reich, N.C. (2005). STAT3 nuclear import is independent of tyrosine phosphorylation and mediated by importin-alpha3. Proc. Natl. Acad. Sci. USA *102*, 8150–8155.

Marti, M., Baum, J., Rug, M., Tilley, L., and Cowman, A.F. (2005). Signal-mediated export of proteins from the malaria parasite to the host erythrocyte. J. Cell Biol. *171*, 587–592.

Marti, M., Good, R.T., Rug, M., Knuepfer, E., and Cowman, A.F. (2004). Targeting malaria virulence and remodeling proteins to the host erythrocyte. Science *306*, 1930–1933.

Menard, R., and Janse, C. (1997). Gene targeting in malaria parasites. Methods *13*, 148–157.

Menard, R., Sultan, A.A., Cortes, C., Altszuler, R., van Dijk, M.R., Janse, C.J., Waters, A.P., Nussenzweig, R.S., and Nussenzweig, V. (1997). Circumsporozoite protein is required for development of malaria sporozoites in mosquitoes. Nature *385*, 336–340.

Myung, J.M., Marshall, P., and Sinnis, P. (2004). The Plasmodium circumsporozoite protein is involved in mosquito salivary gland invasion by sporozoites. Mol. Biochem. Parasitol. *133*, 53–59.

Pied, S., Civas, A., Berlot-Picard, F., Renia, L., Miltgen, F., Gentilini, M., Doly, J., and Mazier, D. (1992). IL-6 induced by IL-1 inhibits malaria pre-erythrocytic stages but its secretion is down-regulated by the parasite. J. Immunol. *148*, 197–201.

Reid, S.P., Leung, L.W., Hartman, A.L., Martinez, O., Shaw, M.L., Carbonnelle, C., Volchkov, V.E., Nichol, S.T., and Basler, C.F. (2006). Ebola virus VP24 binds karyopherin alpha1 and blocks STAT1 nuclear accumulation. J. Virol. *80*, 5156–5167.

Renia, L., Miltgen, F., Charoenvit, Y., Ponnudurai, T., Verhave, J.P., Collins, W.E., and Mazier, D. (1988). Malaria sporozoite penetration. A new approach by double staining. J. Immunol. Methods *112*, 201–205.

Saeij, J.P., Boyle, J.P., Coller, S., Taylor, S., Sibley, L.D., Brooke-Powell, E.T., Ajioka, J.W., and Boothroyd, J.C. (2006). Polymorphic secreted kinases are key virulence factors in toxoplasmosis. Science *314*, 1780–1783.

Saeij, J.P., Coller, S., Boyle, J.P., Jerome, M.E., White, M.W., and Boothroyd, J.C. (2007). Toxoplasma co-opts host gene expression by injection of a polymorphic kinase homologue. Nature *445*, 324–327.

Shapira, S., Harb, O.S., Caamano, J., and Hunter, C.A. (2004). The NF-kappaB signaling pathway: immune evasion and immunoregulation during toxoplasmosis. Int. J. Parasitol. *34*, 393–400.

Short, H.E., Bray, R.S., and Cooper, W. (1954). Further notes on the tissue stages of Plasmodium cynomolgy. Trans. R. Soc. Trop. Med. Hyg. *48*, 122–133.

Stewart, M.J., and Vanderberg, J.P. (1991). Malaria sporozoites release circumsporozoite protein from their apical end and translocate it along their surface. J. Protozool. *38*, 411–421.

Sudbeck, P., and Scherer, G. (1997). Two independent nuclear localization signals are present in the DNA-binding high-mobility group domains of SRY and SOX9. J. Biol. Chem. *272*, 27848–27852.

Taganov, K.D., Boldin, M.P., Chang, K.J., and Baltimore, D. (2006). NF-kappaB-dependent induction of microRNA miR-146, an inhibitor targeted to signaling proteins of innate immune responses. Proc. Natl. Acad. Sci. USA *103*, 12481–12486.

Talcott, B., and Moore, M.S. (2000). The nuclear import of RCC1 requires a specific nuclear localization sequence receptor, karyopherin alpha3/Qip. J. Biol. Chem. *275*, 10099–10104.

Taniguchi, M., Harada, M., Kojo, S., Nakayama, T., and Wakao, H. (2003). The regulatory role of Valpha14 NKT cells in innate and acquired immune response. Annu. Rev. Immunol. *21*, 483–513.

Taylor, S., Barragan, A., Su, C., Fux, B., Fentress, S.J., Tang, K., Beatty, W.L., Hajj, H.E., Jerome, M., Behnke, M.S., et al. (2006). A secreted serine-threonine kinase determines virulence in the eukaryotic pathogen Toxoplasma gondii. Science *314*, 1776–1780.

Tsuji, M., Mattei, D., Nussenzweig, R.S., Eichinger, D., and Zavala, F. (1994). Demonstration of heat-shock protein 70 in the sporozoite stage of malaria parasites. Parasitol. Res. *80*, 16–21.

van de Sand, C., Horstmann, S., Schmidt, A., Sturm, A., Bolte, S., Krueger, A., Lutgehetmann, M., Pollok, J.M., Libert, C., and Heussler, V.T. (2005). The liver stage of Plasmodium berghei inhibits host cell apoptosis. Mol. Microbiol. *58*, 731–742.

Wang, Q., Fujioka, H., and Nussenzweig, V. (2005). Exit of Plasmodium sporozoites from oocysts is an active process that involves the circumsporozoite protein. PLoS Pathog *1*, e9. 10.1371/journal.ppat.0010009.

Weis, K. (2003). Regulating access to the genome: nucleocytoplasmic transport throughout the cell cycle. Cell *112*, 441–451.

Wu, J., Matunis, M.J., Kraemer, D., Blobel, G., and Coutavas, E. (1995). Nup358, a cytoplasmically exposed nucleoporin with peptide repeats, Ran-GTP binding sites, zinc fingers, a cyclophilin A homologous domain, and a leucine-rich region. J. Biol. Chem. *270*, 14209–14213.

Accession Numbers

The data discussed in this publication have been deposited in NCBIs Gene Expression Omnibus (GEO, http://www.ncbi.nlm.nih.gov/geo/) and are accessible through GEO Series accession number GSE8784.